Published in final edited form as:

J Chem Thermodyn. 2016 August ; 99: 54–64. doi:10.1016/j.jct.2016.03.036.

Speed-of-Sound Measurements in (Argon + Carbon Dioxide) over the Temperature Range from (275 to 500) K at Pressures up to 8 MPa

Robin Wegge[†], **Mark O. McLinden**[‡], **Richard A. Perkins**[‡], **Markus Richter**[†,1], and **Roland Span**[†]

[†]Lehrstuhl für Thermodynamik, Ruhr-Universität Bochum, D-44780 Bochum, Germany

[‡]Applied Chemicals and Materials Division, National Institute of Standards and Technology, 325 Broadway, Mailstop 647.07, Boulder, Colorado 80305, United States

Abstract

The speed of sound of two (argon + carbon dioxide) mixtures was measured over the temperature range from (275 to 500) K with pressures up to 8 MPa utilizing a spherical acoustic resonator. The compositions of the gravimetrically prepared mixtures were (0.50104 and 0.74981) mole fraction carbon dioxide. The vibrational relaxation of pure carbon dioxide led to high sound absorption, which significantly impeded the sound-speed measurements on carbon dioxide and its mixtures; pre-condensation may have also affected the results for some measurements near the dew line. Thus, in contrast to the standard operating procedure for speed-of-sound measurements with a spherical resonator, non-radial resonances at lower frequencies were taken into account. Still, the data show a comparatively large scatter, and the usual repeatability of this general type of instrument could not be realized with the present measurements. Nonetheless, the average relative combined expanded uncertainty ($k = 2$) in speed of sound ranged from (0.042 to 0.056)% for both mixtures, with individual state-point uncertainties increasing to 0.1%. These uncertainties are adequate for our intended purpose of evaluating thermodynamic models. The results are compared to a Helmholtz energy equation of state for carbon capture and storage applications; relative deviations of (−0.64 to 0.08)% for the (0.49896 argon + 0.50104 carbon dioxide) mixture, and of (−1.52 to 0.77)% for the (0.25019 argon + 0.74981 carbon dioxide) mixture were observed.

Keywords

argon; carbon capture and storage; carbon dioxide; gas mixture; spherical resonator; speed of sound

1. INTRODUCTION

Knowledge of the thermodynamic properties of CO_2-containing mixtures is essential for the design and operation of carbon capture and storage (CCS) systems, which are being investigated to reduce CO_2 emissions from fossil-fuel power plants. Toward this end,

[1]Corresponding author. Tel.: +49-234-32-26395, m.richter@thermo.rub.de.

Gernert and Span [1] developed the mixture model “Equation of State for Combustion Gases and Combustion-Gas-like Mixtures” (EOS-CG). Although, this mixture model describes most CCS-relevant mixtures better than other available multi component mixture models (*e.g.*, the GERG-2008 equation of state by Kunz and Wagner [2]), further improvements are desirable.

Experimental sound-speed data are particularly useful for developing these equations of state, but there are no sound-speed data available in the literature for the (argon + carbon dioxide) system. To provide data to evaluate and improve the accuracy of the EOS-CG for this system, we investigated the vapor phase (p, c, T, x) behavior of two (argon + carbon dioxide) mixtures. Measurements were made with the spherical acoustic resonator at NIST-Boulder (as described by Perkins and McLinden [3]) over the temperature range from (275 to 500) K with pressures up to 8 MPa. The compositions of the gravimetrically prepared mixtures were (0.50104 and 0.74981) mole fraction carbon dioxide. The measurements included the critical region of the mixtures and points in the vicinity of the dew line. We show comparisons of the measured sound speeds with values calculated from the EOS-CG.

2. EXPERIMENTAL SECTION

2.1. Experimental Material

We prepared the binary gas mixtures gravimetrically using the components described in table 1. The materials were used as received, but we did confirm the purity of the argon with our own analysis.

Gas cylinders (made of aluminum) with an internal volume of approximately 6 L were used. The cylinders were equipped with brass cylinder valves with PTFE gaskets and seats. To remove residual molecules (in particular water) from the cylinders, they were filled with research-grade nitrogen to a pressure of approximately 2 MPa and then evacuated to a very low final pressure $<10^{-4}$ Pa; this purge-evacuate cycle was repeated three times. The sample cylinders were then connected to the carbon dioxide or argon supply cylinder via a manifold, and the sample lines were purged and evacuated three times. The sample cylinder was then placed on a platform balance (with a resolution of 0.1 g), and sample was slowly introduced until the (pre-calculated) target mass was reached. We then disconnected the cylinder from the manifold and utilized a high-precision mass comparator for the determination of the actual sample mass loaded into the cylinder.

The mass of the sample was determined by a double substitution weighing [4], with a nearly identical “tare” or reference cylinder serving as the main substitution mass. The weighing design consisted of four separate weighings: (1) the tare cylinder and standard masses (as needed to bring the mass comparator into its weighing range), (2) the sample cylinder and standard masses, (3) the sample cylinder and masses used in weighing 2 plus a 20 g sensitivity mass (which served to check the linearity of the mass comparator), and (4) the tare cylinder and masses used in weighing 1 plus the sensitivity mass. The key advantage in this approach was that the air buoyancy effect was reduced to the (small) difference in volumes of the tare and sample cylinders and the relatively small effect of the standard masses. The mass comparator used in these measurements had a total capacity of 10060 g,

an electronic weighing range of 60 g, a resolution of 0.1 mg, and a linearity and repeatability of 0.3 mg according to the manufacturer's specification.

The sample cylinders were loaded to a pressure of $p = 7.9$ MPa for the (0.25019 argon + 0.74981 carbon dioxide) mixture and $p = 8.6$ MPa for the (0.49896 argon + 0.50104 carbon dioxide) mixture. The compositions of the two prepared gas mixtures are given in table 2. As discussed in section 2.4, the composition of the sample in the measuring cell could be different from that calculated from the sample masses loaded into the sample cylinder, and we accounted for that in the uncertainty analysis.

2.2. Apparatus Description

Comprehensive descriptions of spherical resonators and the related theory have been reported by Moldover et al. [5], Trusler [6], and others. Additionally, Perkins and McLinden [3] have thoroughly described the spherical acoustic resonator used in the present work. Therefore, we confine the description of both the setup and the theory of the instrument to the details relevant for this work.

The sphere was made up of two thick-walled stainless steel hemispheres (*i.d.*: 80 mm, *o.d.*: 120 mm), which were joined by a twelve-bolt flange with a polyimide gasket as the seal. It was designed as a pressure vessel with a maximum operating pressure of 40 MPa in a temperature range from (80 to 500) K. However, measurements carried out in this work were limited to $p \approx 8$ MPa due to the filling pressure of the sample cylinders, and to a minimum temperature of 275 K resulting from the cooling capabilities of the present thermostat. Filling ports for the inlet and outlet of the sample fluid were located at the poles of the hemispheres. Additionally, ports for the two solid-dielectric, capacitance-type transducers, based on the design of Trusler and Zarari [7], were incorporated into the upper hemisphere. The membrane of both transducers was made of polyimide. The emitter and the receiver transducer were separated by an angle of 90 degrees to reduce interference between the (0, 2) radial mode and the (3, 1) mode.

A vacuum thermostat system with capabilities for fluid cooling (below ambient temperature) and electrical heating (above ambient temperature) provided a uniform and controlled environment for the resonator. By means of the multi-layer-type thermostat, the stability of the temperature at the innermost element (the sphere) was better than 5 mK. A close-fitting, multi-part copper sleeve reduced temperature gradients across the resonator. Two capsule-type 25 Ω standard platinum resistance thermometers (SPRT), calibrated on ITS-90, were used to measure and control the cell temperature. The "cell SPRT," which was used to determine the temperatures reported here, was measured with an alternating-current thermometry bridge (ASL[2], type: F700, UK) against a calibrated 25 Ω reference resistor (thermostated at 310.15 K) manufactured by the company James G. Biddle. The uncertainty ($k = 1$) in temperature measurement was estimated to be 20 mK, including uncertainties in

[2]Certain trade names and products are given to adequately document the experimental equipment and procedures. This does not constitute a recommendation or endorsement of these products by the National Institute of Standards and Technology, nor does it imply that the products are necessarily the best available for the purpose.

the temperature measurement system and uncertainties arising from temperature gradients and oscillations over time.

Pressures were measured with vibrating-quartz-crystal-type pressure transducers (Paroscientific, USA). Depending on the pressure range, one of three transducers, with maximum pressures of 0.7 MPa, 6.2 MPa, and 41 MPa, was used. The pressure transducers were housed in a close-fitting aluminum block, which was thermostated at $T = 313.15$ K to minimize the effects of variations in ambient temperature. Calibrations with a piston gauge are performed annually at NIST-Boulder. Furthermore, the zero drift of the transducers was observed while evacuating the sphere and corrections were applied if necessary. The uncertainty ($k = 1$) in pressure measurement was ($20 \cdot 10^{-6} \cdot p + 0.020$ kPa) for the low-range transducer, ($20 \cdot 10^{-6} \cdot p + 0.15$ kPa) for the mid-range transducer and ($20 \cdot 10^{-6} \cdot p + 1.0$ kPa) for the high-range transducer.

2.2.1. Speed-of-Sound Measurement Procedure—To measure the speed of sound, the emitter transducer was excited by a sinusoidal excitation voltage provided by a synthesized function generator (Stanford Research Systems, type: DS345, USA) and amplified by an audio transformer. The polarized receiver transducer generated a voltage as sound waves moved its membrane. The receiver output was connected with a triaxial cable to a bootstrapped JFET operational amplifier (see Trusler [6], and Perkins and McLinden [3] for details). A digital lock-in amplifier (EG&G, type: 7260, USA) recorded this output as in-phase and quadrature signals. Typically, a measurement consisted of a series of frequency scans, with both increasing and decreasing frequency, centered around the first three to five radial modes. The consistency of the measurements could be checked by (1) comparing the results for increasing and decreasing frequency scans (differences may indicate, *e.g.*, an insufficient settling time for a frequency increment or problems with dispersion effects), (2) comparing the results calculated for the individual modes, and (3) comparisons of the replicates of these frequency scans.

The process of finding and measuring the resonance peaks has been largely automated by Perkins and McLinden [3]. The assumption of their peak-finding algorithm is that the relative position of the peaks in the complex spectrum of resonances scales with the sound speed of the fluid under investigation. Hence, by locating the position of one peak, the frequency of the other peaks can be estimated. Usually, estimated peak locations are based on the lowest radial mode (0, 2). Using equation 1 (see below) and a (preliminary) equation of state to calculate the speed of sound, the resonance frequency of any specified mode can be estimated. This estimation is sufficient to find the first peak, and, based on the measured value of the first peak's resonance frequency, all subsequent peaks are automatically located by the peak-finding algorithm.

2.2.2. Influence of Carbon Dioxide on the Measurements—For the measurements carried out in this work, the peak-finding algorithm often did not yield satisfactory results. To investigate the cause, we measured resonance spectra over a wide range of frequencies for argon, carbon dioxide, and two (argon + carbon dioxide) mixtures at several different temperatures and pressures; four of these spectra are shown in figure 1. In figure 1(a), a spectrum of resonances for a non-dispersive gas (argon) is shown. A good

signal-to-noise ratio over the whole frequency range can be observed, and, in the enlarged detail, a distinct resonance peak for the (0, 2) mode can be seen. It is important to note that broad peaks from the resonator system itself are present over the frequency range from (3.0 to 4.6) kHz, but these frequencies lie below the (0, 2) mode in argon, and the measurement is not affected. Perkins and McLinden [3] estimated the breathing frequency of the resonator sphere to be in the range of (20 to 24) kHz; we could not identify the specific source of the signals in the (3.0 to 4.6) kHz range.

For carbon dioxide (*cf.* figure 1(b)), however, the speed of sound is lower than that of pure argon, and the (0, 2) mode overlaps the resonances of the system, and there is a more efficient coupling between the gas and the resonator itself. The result is that the (0, 2) gas resonance is nearly lost in the noise, and the nearby (3, 1) peak is very broad. Moldover et al. [5] discuss this peak-broadening effect when gas resonances overlap system resonances. The location of the (0, 2) resonance could be found only because a nearly exact starting point for the peak-finding algorithm could be calculated with the reference equation of state for carbon dioxide of Span and Wagner [8]. For the (argon + carbon dioxide) mixture (*cf.* figure 1(c)), the (0, 2) mode is completely obscured. (Because of these problems, no useful data could be obtained from the spectra shown in Figure 1(c), and no data are reported for p = 0.5 MPa for the isotherm at 275 K.) Figures 1(b) and 1(c) represent examples of worst-case conditions. A more typical result for the majority of our measurements is shown in figure 1(d). But, even here, the (0, 2) mode is observable only as a shoulder on the leading edge of the (3, 1) peak.

Because of the overlap of the (0, 2) mode with the system resonances, this mode was completely dropped from the analysis. The (1, 1) mode for argon, carbon dioxide and the mixtures, on the other hand, is located at frequencies below this problematic region. Thus, as proposed by Estrada-Alexanders and Trusler [9], the measurements were based on the first non-radial mode (1, 1). This mode is quite distinct in the spectra of carbon dioxide and the (argon + carbon dioxide) mixtures. The peak-finding algorithm was modified to first find the (1, 1) mode and then estimate the frequencies of the other modes based on it. Because of the distinct (1, 1) mode, reliable starting values for the (0, 3) and (0, 4) modes could be calculated, and the peak-finding algorithm located those modes most of the time.

2.2.3. Determination of Sound Speed—The sound speed c of the fluid was determined by

$$f_{ln}+ig_{ln}=\nu_{ln}\left(\frac{c}{2\pi r}\right)\sum_j(\Delta f+ig), \quad (1)$$

where the speed of sound c is related to the resonance frequency f_{ln} and the half-width g_{ln} of the resonance peak (both experimentally determined), to the eigenvalues ν_{ln} of the spherical Bessel function, and the sphere radius r. The subscript ln refers to the order of the resonances. The effective radius of the sphere was calibrated as a function of temperature and pressure with sound-speed measurements in high-purity argon; this procedure is

described in detail by Perkins and McLinden [3]. The summation over *j* accounts for small corrections, such as for the thermal boundary layer, the coupling between the gas and the shell motion, the fluid dispersion/sound absorption, and the perturbation of the resonance frequency by the filling tubes and the emitter and receiver transducers.

Vibrational relaxation in carbon dioxide is severe. As reported by *e.g.*, Kneser and Roesler [10] and Simpson et al. [11], this effect is further pronounced in mixtures of argon and carbon dioxide. Hence, the resulting correction for dispersion must be carefully considered. Generally, Kneser and Roesler [10] propose to approximate the isothermal vibrational relaxation time of a mixture of a relaxing and a non-relaxing gas by

$$\frac{1}{\tau_m}=\frac{x_1}{\tau_{11}}+\frac{(1-x_1)}{\tau_{12}}, \quad (2)$$

where x_1 is the mole fraction of the relaxing species, τ_{11} is the vibrational relaxation time of the pure relaxing gas, τ_{12} is the relaxation time arising from unlike collisions, and τ_m is the resulting isothermal vibrational relaxation time of the mixture. However, the relaxation times used in the present vibrational dispersion correction could be retrieved directly from the publications of Kneser and Roesler [10] and Simpson et al. [11]. Kneser and Roesler [10] studied the sound absorption in (argon + carbon dioxide) mixtures over a wide composition range at T = 296.15 K. Additionally, Simpson et al. [11] studied the sound absorption of a (0.9 argon + 0.1 carbon dioxide) mixture up to temperatures of T = 3000 K; from that data set the temperature dependence of the vibrational relaxation times given by Kneser and Roesler [10] could be derived.

Furthermore, the dispersion effect of damped concentration fluctuations must also be considered for mixtures (*cf.* Moldover and Mehl [5] and Estrada-Alexanders and Trusler [12]). Estrada-Alexanders and Trusler [12] found that the effects of both rotational relaxation and damped concentration fluctuations were small compared to those of vibrational relaxation for mixtures of ethane with carbon dioxide. Thus, only the correction for vibrational dispersion is applied in the present mixture measurements. The largest dispersion corrections were calculated for data points measured at low temperatures and low pressures. At these points the corrections were approximately 1% of the measured resonance frequency. Nevertheless, in large areas of the investigated pressure and temperature range the corrections were smaller than 0.05%.

The described corrections for equation 1 are well known for the radial modes, but the corrections are much more complicated and are not readily reduced to simple expressions for non-radial modes [6]. The general behavior is similar to the radial case and, as a first approximation, the corrections for the radial resonances were also applied to the non-radial modes. Furthermore, non-radial resonances are affected by viscous damping. Combining the expressions from Moldover et al. [5], Trusler [6] and Goodwin et al. [13], the influence Δf_v of the viscous boundary layer on the resonance frequency can be approximated by

$$\Delta f_{\mathrm{v}} = -g_{\mathrm{v}} \left(1 - \left(\frac{2l_{\mathrm{v}}}{\delta_{\mathrm{v}}}\right)\right). \quad (3)$$

Additionally, the influence g_{v} on the half-width of the resonance peak

$$g_{\mathrm{v}} = (\gamma - 1) \left(\frac{f_{jn}}{2r}\right) \delta_{\mathrm{v}} \quad (4)$$

must be corrected. In these equations γ is the ratio of constant pressure heat capacity C_p to constant volume heat capacity C_v, and f_{jn} is the measured resonance frequency; δ_{v} denotes the viscous penetration length, which is defined by

$$\delta_{\mathrm{v}} = \sqrt{\frac{\eta}{\rho \pi f_{ln}}}, \quad (5)$$

where η is the dynamic viscosity and ρ is the density of the fluid. Finally, l_{v} describes the viscous accommodation length, which is given by

$$l_{\mathrm{v}} = \left(\frac{\eta}{p}\right) \sqrt{\frac{\pi RT}{M}} \left(\frac{2 - h_{\mathrm{v}}}{h_{\mathrm{v}}}\right). \quad (6)$$

Here, p and T are the pressure and temperature at the particular state point. M is the molar mass of the gas, R is the molar gas constant, and h_{v} is the viscous accommodation coefficient. Because of a lack of data, we assume $h_{\mathrm{v}} = 1$ in this work. The thermodynamic properties needed for the above-described corrections could be calculated with sufficient accuracy employing the EOS-CG of Gernert and Span [1]. The required transport properties were estimated for the mixtures with REFPROP 9.1 [14] based on the extended corresponding states models described by Huber et al. [15] and assessed by Chichester and Huber [16].

In a perfect sphere, the (1, 1) non-radial resonance peak is a three-component degenerate multiplet. Estrada-Alexanders and Trusler [9] report that geometric imperfections are usually sufficient to obtain three partially-resolved components and describe a procedure to model the multiplet as the superposition of three Lorentzian-type functions plus a constant background term to calculate a mean frequency. Additionally, they suggest performing calibration measurements in argon at temperatures where the frequencies of the argon modes are close to those that would be encountered during the measurements. Neither approach could be realized for the present measurements. Due to the high sphericity of our resonator, the (1, 1) peak could not be resolved into three components. Calibration measurements in argon at carbon dioxide-like frequencies would have required cooling the cell to T = 170 K,

which was below the lower temperature limit of the thermostat. The consequences arising from these limitations will be discussed in section 3.

2.3. Experimental Procedures

Measurements were carried out along isotherms. Prior to the mixture measurements, the calibration of the effective radius of the sphere was checked with measurements in high-purity argon; no significant deviations to the calibration performed by Perkins and McLinden [3] were observed. Subsequently, the system was thoroughly evacuated and, with the set-point temperature set to the lowest temperature and the sample cylinder connected to the sample manifold, the first (argon + carbon dioxide) mixture under study (0.50104 mole fraction carbon dioxide) was filled into the evacuated sphere to a pressure of 0.5 MPa. After 15 minutes, the sample was vented and the system was evacuated for 5 minutes. This purge-evacuate cycle was repeated three times before the sphere was pressurized to the maximum filling pressure of the sample cylinder, which was approximately 8 MPa. As soon as the sphere temperature was stable within acceptable limits ($\sigma_T \leq 2$ mK), an additional 60 minutes were allowed before the frequency scans started. Further isothermal (T, p) state points at lower pressures followed (with a similar equilibration time allowed) until the minimum pressure of 0.5 MPa was reached. Due to the increasing sound absorption with decreasing pressure, attempts to measure below this pressure did not yield any useful results.

After finishing the measurements along an isotherm, the temperature was increased and the sphere was again pressurized to 8 MPa. Due to the high thermal mass of the sphere and the enclosing copper sleeve, measurements in the second (argon + carbon dioxide) mixture (0.74981 mole fraction carbon dioxide) started at the highest set-point temperature and temperatures were decreased for subsequent isotherms.

2.4. Absorption of Carbon Dioxide in Polymeric Materials

Since the sealing gaskets and the transducer membranes were made from polyimide, it is very likely that a significant amount of carbon dioxide was absorbed in these parts during the measurements. The setup of the sample manifold did not enable isobaric purging of the sphere with fresh sample gas during the measurements as suggested by Richter and Kleinrahm [17]. Instead, the sphere was loaded with fresh sample between the isotherms, applying the previously described purge-evacuate cycles. Thus, a shift in composition during a single isotherm might have occurred. To investigate this possibility, we carried out check measurements in high-purity argon after finishing the mixture measurements. As a result of carbon dioxide diffusing out of the gaskets, the experimental sound speeds (at constant temperature and pressure) changed by 0.024% over a time span of approximately 72 h. We assume, that the effect of the diffusion of CO_2 into the gaskets is comparable during a single isotherm, and therefore enlarged the uncertainty for the sample composition of the gravimetrically prepared mixtures to 0.02% ($k = 1$) in speed of sound.

3. RESULTS AND COMPARISON TO THE EOS-CG

3.1. Measured Data

The speed of sound in two (argon + carbon dioxide) mixtures was measured over the temperature range of (275 to 500) K with pressures up to 8 MPa; “mixture 1” had a composition of 0.50104 mole fraction carbon dioxide, and “mixture 2” had a composition of 0.74981 mole fraction carbon dioxide. Measurements were carried out at five (T, p) state points along each of five isotherms at T = (274.99, 299.92, 350.01, 400.20, and 500.47) K for mixture 1, and at five (T, p) state points along each of six isotherms at T = (276.09, 290.01, 310.01, 350.01, 400.13, and 500.48) K for mixture 2. These included measurements in the critical region and in the vicinity of the dew line. As described above, a single measurement consisted of a series of frequency scans with increasing and decreasing frequency, centered around the first non-radial mode (1, 1) and the radial modes (0, 3) and (0, 4). Moreover, multiple replicates were measured at every (T, p) state point, leading to a total of 385 (p, c, T, x) data points for mixture 1 and 459 *(p, c, T, x)* data points for mixture 2; these are all tabulated in the supplemental data.

The usually good repeatability of measurements with this instrument could not be achieved in this series of measurements. Therefore, for both mixtures an averaged data set has been calculated, disregarding a relatively high number of outliers. (Data points, which were not considered for averaging are printed in italics within the tables in the supplemental data.) We report 67 averaged (p, c, T, x) data for mixture 1 and 82 averaged (p, c, T, x) data for mixture 2, which are listed in tables 3 and 4 and depicted in figures 2 and 3.

3.2. Uncertainty

A detailed uncertainty analysis for our instrument was provided by Perkins and McLinden [3]; this analysis is only valid for sound speeds calculated from radial resonances. For non-radial modes, additional uncertainty contributions, *e.g.*, accounting for the viscous damping, would be necessary. A complete description of the uncertainties for non-radial modes is not available in the literature and is outside the scope of this work. We assumed that the uncertainty analysis for the non-radial and the radial modes are identical for the present measurements, except that the uncertainty due to the boundary layers was increased to 5% (k = 1) for the non-radial modes, to also account for the viscous damping. Ultimately, this increased contribution did not greatly affect the combined uncertainty. Rather, the contributions arising from the uncertainty in the mixture composition and the uncertainties due to broad peaks had the greatest impact, but these effects were already included in the analysis of Perkins and McLinden [3]. Our final estimate for the average relative combined expanded uncertainty (k = 2) for the measurements ranged from (0.042 to 0.056)% for the two mixtures, with individual state-point uncertainties going up to 0.1% (mainly due to broad peaks).

3.3. Comparison to the EOS-CG

In tables 3 and 4, we also report the relative deviations of the experimental speeds of sound from values calculated with the EOS-CG equation of state by Gernert and Span [1]. Since no experimental sound-speed data were available during the fitting procedure, the authors of

this equation do not report uncertainties for sound speed in (argon + carbon dioxide) mixtures. In figures 4 and 5, the results of the measurements with mixture 1 and mixture 2 are shown. Relative deviations of the present data from values calculated with the EOS-CG equation of state are plotted versus pressure. As mentioned above, the vibrational relaxation of carbon dioxide impeded the measurements. The resulting high sound absorption varied with frequency, and therefore the results for the three measured modes show a comparatively high deviation with each other in regions of high sound absorption. Especially at the lower temperatures, significant differences between the non-radial and the radial modes of up to 0.15% for mixture 1 and up to 0.25% for mixture 2 were observed. In contrast, at higher temperatures the deviations between the non-radial and the radial modes decrease and are, for temperatures above 350 K, mostly within the experimental uncertainty. Nevertheless, an offset between the non-radial and the radial modes over the entire temperature range can be seen, which may be due to the incomplete corrections for the non-radial modes. Hence, the sound speeds calculated from radial resonances should be considered as the more reliable data set, and therefore we recommend them for purposes such as fitting equations of state.

The sound absorption of carbon dioxide increases with decreasing pressure. Thus, measurements at pressures below 0.5 MPa did not yield any satisfactory results for the radial modes. At pressures of the order of 0.1 MPa, the sound absorption was so pronounced that even the measurements of the (1, 1) mode did not yield any usable results and, hence, are not reported here.

Independent of the modes, at temperatures above 350 K, the equation of state shows good agreement with our experimental data for both mixtures (see figures 4 and 5). No additional experimental speed-of-sound data for (argon + carbon dioxide) mixtures were found in the literature.

3.4. Potential Pre-Condensation in the Vicinity of the Dew Line

At lower temperatures, in the vicinity of the dew line and in the critical region, relatively large deviations (up to −1.52%) compared to the EOS-CG can be observed. Comparable trends have been observed in speed-of-sound measurements on pure gases with spherical and cylindrical resonators by, *e.g.*, Younglove and McCarty [18] and Mehl and Moldover [19]. Mehl and Moldover [19] have identified a sharp, anomalous decrease of the apparent speed of sound near the dew line ($p \approx 0.9\ p_S$) in the nitrogen measurements by Younglove and McCarty [18] and reproduced this general behavior with measurements in propane. The magnitude of this effect was as large as several percent in speed of sound. The observed phenomenon is described by Mehl and Moldover [19] as pre-condensation on the inner surface of the resonator. They report a model to calculate the change in the specific acoustic admittance, caused by a liquid film on a smooth wall. This pre-condensation is more complex for the mixtures under study here since carbon dioxide will preferentially condense on the wall and further condensation becomes diffusion limited. The mixture case has been explored by Swift and Spoor [20].

In the present work, only the measurements in mixture 2 at $T = 276.09$ K and $p > 5$ MPa correspond to pressures grater than $0.9\ p_S$ (see figure 5, panel 1). Measurements in mixture 1 at $T = 274.99$ K and $p > 6$ MPa and measurements in mixture 2 at $T = 276.09$ K and $p > 4$

MPa, at T = 290.01 K and p > 6 MPa, and at T = 310.01 K and p = 8.06 MPa correspond to temperatures smaller than 1.1 T_S (see figure 4, panel 1 and figure 5, panels 1, 2, and 3). The mechanism described by Mehl and Moldover [19] can be applied to our own data, but there are differences. Mehl and Moldover [19] suggest that pre-condensation is most pronounced at low frequencies and in resonators with rough walls. Our spherical resonator has an inner surface that was polished to a to a mirror-like finish. Furthermore, referring, *e.g.*, to the first panel of figure 5, it can be observed that the results for the mode at the lowest frequency (see diamonds in figure 5 for mode (1, 1); $f_{1,1} \approx 1.93$ kHz) are less affected by potential pre-condensation than the higher frequencies (see rectangles for mode (0, 3) and triangles for mode (0, 4); $f_{0,3} \approx 7.14$ kHz and $f_{0,4} \approx 10.1$ kHz). Measurements at high frequencies (f > 1 MHz) were proposed by Mehl and Moldover [19] to avoid pre-condensation; such frequencies are beyond the limits of our apparatus and have not been tested in this work. Hence, pre-condensation in close proximity to the dew line cannot be excluded.

It was shown recently by Westman et al. [21] that the EOS-CG equation of state by Gernert and Span [1] shows large deviations to experimental data for the (nitrogen + carbon dioxide) system in the vicinity of the phase boundary and especially in the critical region. This observation is consistent with the present measurements on (argon + carbon dioxide) mixtures, since comparably large deviations (up to −0.19%) can be observed at a relatively large distance to the dew line ($p \approx 0.8\ p_S$). Thus, a superposition of pre-condensation effects and a weakness in the EOS-CG is the most probable explanation of the observed deviations. However, without further detailed investigations it is not possible to judge which of these issues is the dominant one. Accordingly, the data points which are potentially affected by pre-condensation are marked in the deviation plots and tables (see red symbols in figures 4 and 5 and values printed in italics in tables 3 and 4).

4. CONCLUSIONS

Accurate (p, c, T, x) data were measured for two (argon + carbon dioxide) mixtures (with mole fractions of 0.50104 and 0.74981 carbon dioxide) utilizing a spherical acoustic resonator [3]. The vibrational relaxation of carbon dioxide significantly impeded the measurements carried out in this work; pre-condensation may have also affected the data measured close to the dew line. In contrast to the standard operating procedure for speed-of-sound measurements with a spherical resonator, non-radial resonances at lower frequencies were also measured. As proposed by Estrada-Alexanders and Trusler [9], the measurements were based on the first non-radial mode (1, 1). On basis of the measured value for this mode, the radial resonances (0, 3) and (0, 4) were measured automatically, utilizing the peak-finding algorithm by Perkins and McLinden [3]. Because of the high sphericity of the spherical resonator utilized and a restricted lower temperature limit of the thermostat, not all corrections for non-radial modes proposed by Estrada-Alexanders and Trusler [9] could be applied to the present measurements. Therefore, an offset between the sound speeds derived from the non-radial and the radial modes was observed, although, at temperatures above 350 K this offset lies within the experimental uncertainty of the present measurements. The measurements were carried out over the temperature range from (275 to 500) K with pressures up to 8 MPa with an estimated average relative combined expanded uncertainty (k

= 2) in speed of sound of (0.042 to 0.056)% for the two mixtures, with individual state-point uncertainties going up to 0.1% (mainly caused by broad peaks).

The experimental sound-speed data for the (argon + carbon dioxide) mixtures were compared to values calculated with the EOS-CG equation of state by Gernert and Span [1]. For this equation the authors do not report an uncertainty in speed of sound for the mixtures studied here. Relative deviations from the EOS-CG of (−0.64 to 0.08)% for the mixture with 0.50104 mole fraction carbon dioxide, and relative deviations of (−1.52 to 0.77)% for the mixture with 0.74981 mole fraction carbon dioxide were observed. The largest deviations were observed in the vicinity of the dew line and in the critical region; this is likely a superposition of pre-condensation [19] and the inaccuracy of the EOS-CG in the vicinity of the dew line. However, our experimental data show reasonable agreement with the equation in the supercritical region. We conclude that our experimental data could be used to optimize the currently available equations of state in the investigated temperature and pressure range.

Supplementary Material

Refer to Web version on PubMed Central for supplementary material.

Acknowledgments

Robin Wegge's work at Ruhr-Universität Bochum, Germany, and his stay at the National Institute of Standards and Technology (NIST) in Boulder (CO), USA, were supported by the research programme CLIMIT and the BIGCCS Centre, performed under the Norwegian research programme Centres for Environment-friendly Energy Research (FME). Robin Wegge acknowledges the following partners for their contributions: Gassco, Shell, Statoil, Total, Engie and the Research Council of Norway (193816/S60 and 200005/S60). We thank Dr. Thomas J. Bruno of NIST for analyzing our argon sample.

References

1. Gernert J, Span R. EOS-CG: A Helmholtz energy mixture model for humid gases and CCS mixtures. J Chem Thermodyn. 2016; 93:274–293.
2. Kunz O, Wagner W. The GERG-2008 wide-range equation of state for natural gases and other mixtures: An expansion of GERG-2004. J Chem Eng Data. 2012; 57:3032–3091.
3. Perkins RA, McLinden MO. Spherical resonator for vapor-phase speed of sound and measurements of 1,1,1,2,2,3,3-heptafluoro-3-methoxypropane (RE347mcc) and trans-1,3,3,3-tetrafluoropropene [R1234ze(E)]. J Chem Thermodyn. 2015; 91:43–61.
4. Harris, GL.; Torres, JA. Selected Laboratory and Measurement Practices and Procedures to Support Basic Mass Calibrations; NISTIR 6969. National Institute of Standards and Technology; Gaithersburg, MD: 2003.
5. Moldover MR, Mehl JB, Greenspan M. Gas-filled spherical resonators: Theory and experiment. J Acoust Soc Am. 1986; 79:253–272.
6. Trusler, JPM. Physical Acoustics and Metrology of Fluids. Adam Hilger; Bristol: 1991.
7. Trusler JPM, Zarari M. The speed of sound and derived thermodynamic properties of methane at temperatures between 275 K and 375 K and pressures up to 10 MPa. J Chem Thermodyn. 1992; 24:973–991.
8. Span R, Wagner W. A new equation of state for carbon dioxide covering the fluid region from the triple-point temperature to 1100 K at pressures up to 800 MPa. J Phys Chem Ref Data. 1996; 25:1509–1596.
9. Estrada-Alexanders AF, Trusler JPM. Speed of sound in carbon dioxide at temperatures between (220 and 450) K and pressures up to 14 MPa. J Chem Thermodyn. 1998; 30:1589–1601.

10. Kneser HO, Roesler H. Die Schallabsorption in CO_2-Ar-Mischungen (The Sound Absorption in CO_2-Ar Mixtures). Acustica. 1959; 9:224–226.
11. Simpson CJSM, Chandler TRD, Strawson AC. Vibrational Relaxation in CO_2 and CO_2-Ar Mixtures Studied Using a Shock Tube and a Laser-Schlieren Technique. J Chem Phys. 1969; 51:2214–2219.
12. Estrada-Alexanders AF, Trusler JPM. Speed of sound in $(0.4C_2H_6 + 0.6CO_2)$ at temperatures between $T = 220$ K and $T = 450$ K and pressures up to $p = 1.2$ MPa. J Chem Thermodyn. 1999; 31:685–695.
13. Goodwin, ARH.; Marsh, KN.; Wakeham, WA. Measurement of the thermodynamic properties of single phases. Elsevier; Amsterdam: 2003.
14. Lemmon, EW.; Huber, ML.; McLinden, MO. Standard Reference Data Program. National Institute of Standards and Technology; Gaithersburg, MD: 2013. NIST Standard Reference Database 23, NIST Reference Fluid Thermodynamic and Transport Properties–REFPROP, Version 9.1.
15. Huber ML, Laesecke A, Perkins RA. Model for the Viscosity and Thermal Conductivity of Refrigerants, Including a New Correlation for the Viscosity of R134a. Ind Eng Chem Res. 2003; 42:3163–3178.
16. Chichester, JC.; Huber, ML. NISTIR 6650. National Institute of Standards and Technology; Jun. 2008 Documentation and Assessment of the Transport Property Model for Mixtures Implemented in NIST REFPROP (Version 8.0).
17. Richter M, Kleinrahm R. Influence of adsorption and desorption on accurate density measurements of gas mixtures. J Chem Thermodyn. 2014; 74:58–66.
18. Younglove BA, McCarty RD. Speed-of-sound measurements for nitrogen gas at temperatures from 80 to 350 K and pressures up to 1.5 MPa. J Chem Thermodyn. 1980:1121–1128.
19. Mehl JB, Moldover MR. Pre-condensation phenomena in acoustic measurements. J Chem Phys. 1982:455–465.
20. Swift GW, Spoor PS. Thermal diffusion and mixture separation in the acoustic boundary layer. J Acoust Soc Am. 1999; 106:1794–1800.
21. Westman SF, Stang HGJ, Løvseth SW, Austegard A, Snustad I, Størset SØ, Ertesvåg IS. Vapor-liquid equilibrium data for the carbon dioxide and nitrogen (CO_2+N_2) system at the temperatures 223, 270, 298 and 303 K and pressures up to 18 MPa. Fluid Phase Equilib. 2015; 409:207–241.

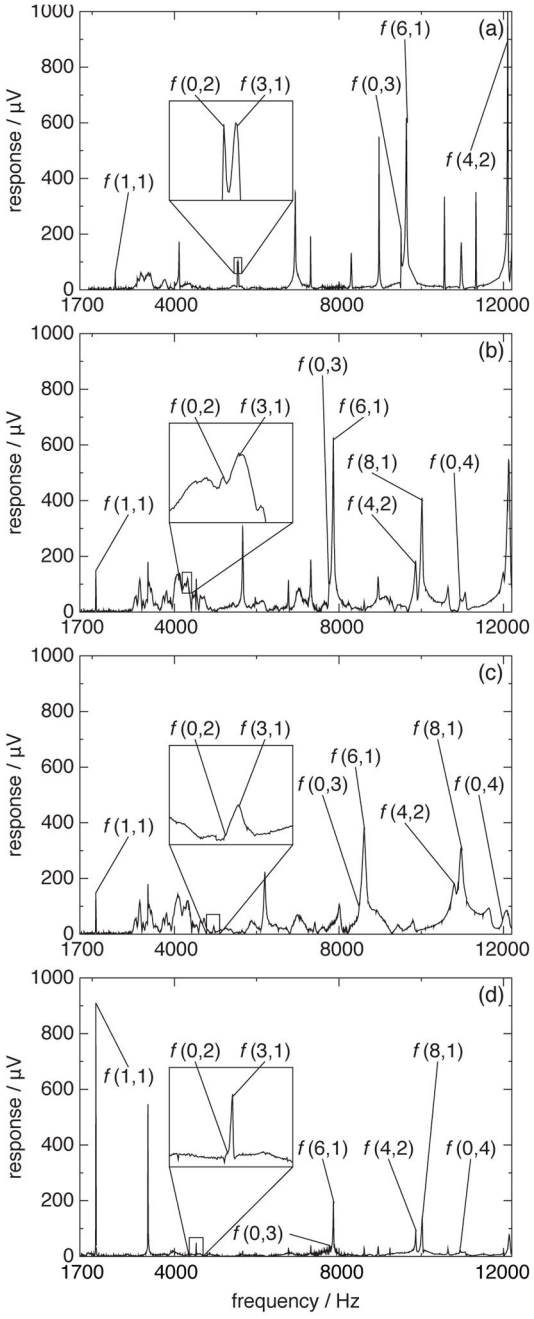

Figure 1.

Spectra of resonances of (a) pure argon (T = 275 K; p = 0.11 MPa), (b) pure carbon dioxide (T = 275 K; p = 0.8 MPa), (c) an (0.49896 argon + 0.50104 carbon dioxide) mixture (T = 275 K; p = 0.5 MPa), and (d) an (0.25019 argon + 0.74981 carbon dioxide) mixture (T = 290 K; p = 4.0 MPa).

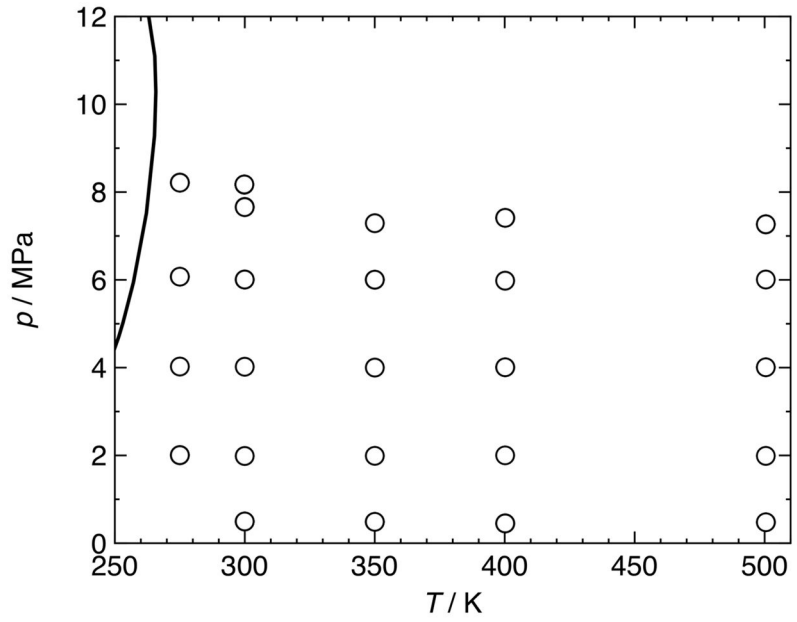

Figure 2.

(*p, T*)-diagram with phase boundary of a (0.49896 argon + 0.50104 carbon dioxide) mixture as calculated with the EOS-CG equation of state of Gernert and Span [1]; ○, (*p, c, T, x*) state points measured in the present work.

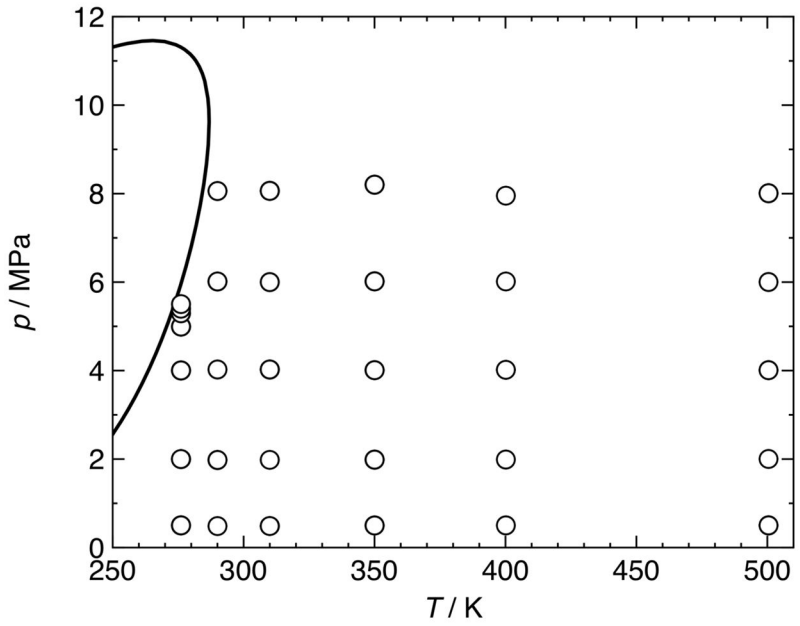

Figure 3.

(*p*, *T*)-diagram with phase boundary of a (0.25019 argon + 0.74981 carbon dioxide) mixture as calculated with the EOS-CG equation of state of Gernert and Span [1]; ○, (*p*, *c*, *T*, *x*) state points measured in the present work.

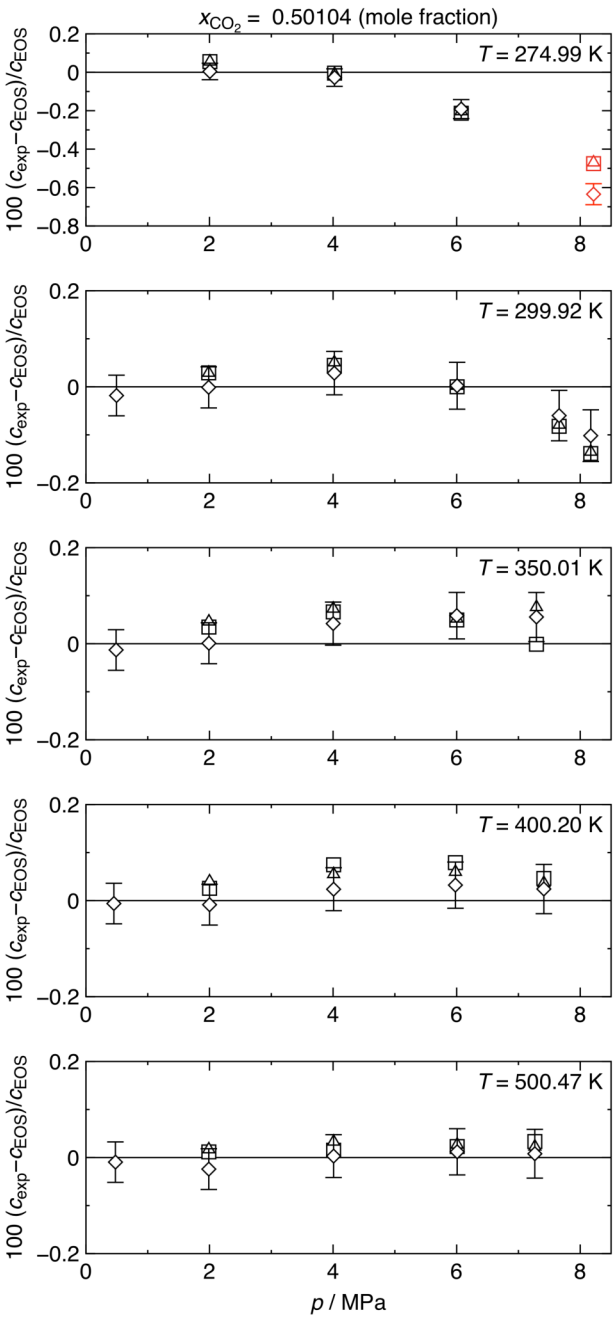

Figure 4.

Results of speed-of-sound measurements in a (0.49896 argon + 0.50104 carbon dioxide) mixture. Relative deviations of experimental speeds of sound c_{exp} from values c_{EOS} calculated with the EOS-CG equation of state of Gernert and Span [1] are plotted versus pressure p. ◇, non-radial mode (1, 1) (including error bars for (0.042 to 0.055)% measurement uncertainty, $k = 2$); △, radial mode (0, 3); □, radial mode (0, 4). Symbols plotted in red indicate points that may have been affected by pre-condensation.

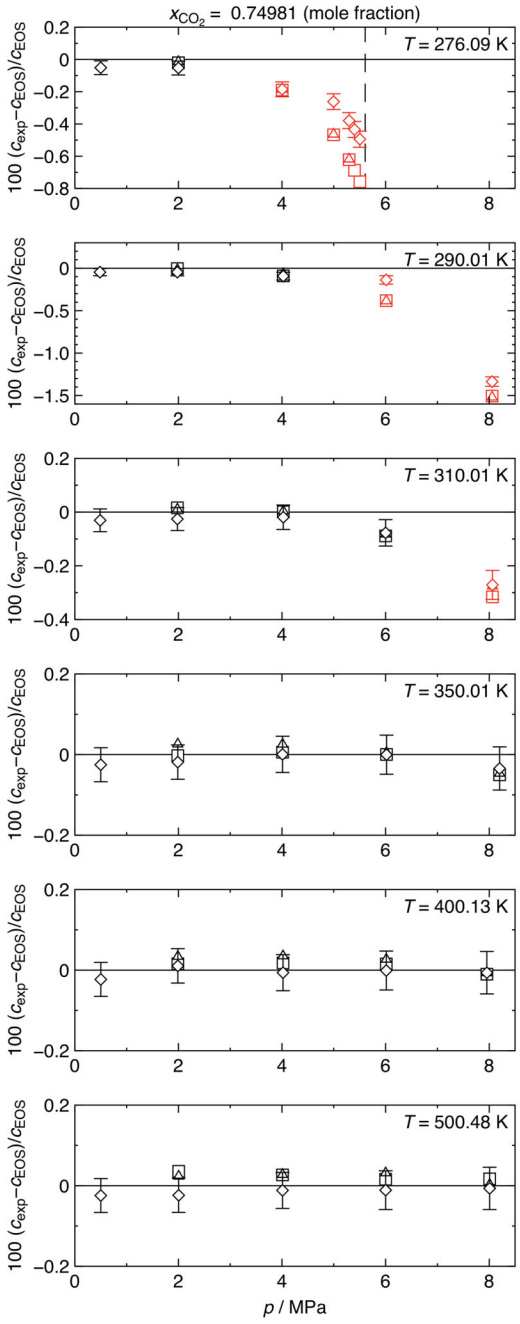

Figure 5.

Results of speed-of-sound measurements in a (0.25019 argon + 0.74981 carbon dioxide) mixture. Relative deviations of experimental speeds of sound c_{exp} from values c_{EOS} calculated with the EOS-CG equation of state of Gernert and Span [1] are plotted versus pressure p. ◇, non-radial mode (1, 1) (including error bars for (0.042 to 0.056)% measurement uncertainty, $k = 2$); △, radial mode (0, 3); □, radial mode (0, 4); ---, phase boundary. Symbols plotted in red indicate points that may have been affected by pre-condensation.

Table 1

Sample information.

Chemical Name	Source	Initial Purity/mole frac.	Purification Method	Final Purity/mole frac.	Analysis Method
argon	Matheson	0.999999	none	0.999999	GC/MS[a]
carbon dioxide	Scott	0.99997	none	-	none

[a]Gas chromatography/mass spectrometry

Table 2

Gravimetric compositions (mole fraction), average molar mass, and standard uncertainty of the molar mass of the studied mixtures.

	Mixture	
Component	**(1)**	**(2)**
argon	0.49896	0.25019
carbon dioxide	0.50104	0.74981
M/g·mol^{-1}	41.983	42.994
$U(M)$/g·mol	0.000022	0.000018

Table 3

Experimental (p, c, T, x) data in the vapor phase for a (0.49896 argon + 0.50104 carbon dioxide) mixture, relative deviations of the experimental data c_{exp} from speeds of sound c_{EOS} calculated with the EOS-CG equation of state of Gernert and Span [1], and the combined expanded uncertainty U_c ($k = 2$) of the speed-of-sound measurements are listed. The results for the non-radial mode $f(1, 1)$ and the radial modes $f(0, 3)$ and $f(0, 4)$ are tabulated individually. p is the pressure and T is the temperature (ITS-90). The standard uncertainty in temperature was less than 20 mK, the standard uncertainty in pressure was ($20 \cdot 10^{-6} \cdot p + 0.15$ kPa) for $p < 5$ MPa and ($20 \cdot 10^{-6} \cdot p + 1.0$ kPa) for $p > 5$ MPa, and the standard uncertainty in mixture composition was $5.5 \cdot 10^{-6}$ (mole fraction). Values written in italics indicate points that may have been affected by pre-condensation.

p/MPa	T/K	c_{exp}/m s^{-1}	$100\left(\frac{c_{exp}-c_{EOS}}{c_{EOS}}\right)$	$U_c(c)$ c^{-1}/%
		$f(1, 1)$		
8.21626	*274.997*	*253.759*	*−0.6346*	*0.0547*
6.07333	274.991	258.012	−0.1916	0.0494
4.02321	274.990	263.855	−0.0277	0.0455
2.00644	275.002	270.444	0.0044	0.0429
		$f(0, 3)$		
8.21534	*274.997*	*254.183*	*−0.4691*	*0.0627*
6.07286	274.991	257.986	−0.2021	0.0544
4.02293	274.990	263.909	−0.0076	0.0463
2.00627	275.001	270.593	0.0597	0.0482
		$f(0, 4)$		
8.21531	*274.997*	*254.168*	*−0.4748*	*0.0560*
6.07288	274.991	257.961	−0.2119	0.0515
4.02295	274.991	263.924	−0.0020	0.0498
2.00629	275.003	270.607	0.0645	0.0699
		$f(1, 1)$		
8.17071	299.845	275.134	−0.1017	0.0538
7.65893	299.956	275.437	−0.0597	0.0525
6.00792	299.948	276.819	0.0023	0.0488
4.02077	299.945	279.772	0.0286	0.0452
1.98696	299.945	283.785	−0.0009	0.0428
0.494360	299.948	287.266	−0.0138	0.0423
		$f(0, 3)$		
8.17018	299.847	275.044	−0.1349	0.0580

p/MPa	T/K	c_{exp}/m s^{-1}	$100\left(\frac{c_{exp}-c_{EOS}}{c_{EOS}}\right)$	$U_c(c)$ c^{-1}/%
7.65802	299.949	275.380	−0.0786	0.0542
6.00747	299.948	276.821	0.0025	0.0511
4.02049	299.946	279.838	0.0518	0.0465
1.98682	299.944	283.882	0.0332	0.0716
		$f(0, 4)$		
8.17009	299.846	275.034	−0.1382	0.0613
7.65792	299.947	275.370	−0.0816	0.0540
6.00748	299.949	276.817	0.0010	0.0493
4.02050	299.946	279.824	0.0466	0.0513
1.98682	299.942	283.891	0.0368	0.0547
		$f(1, 1)$		
7.29116	350.009	306.194	0.0556	0.0512
6.00259	350.009	305.940	0.0584	0.0484
4.00152	350.010	306.296	0.0419	0.0449
1.98998	350.009	307.457	0.0012	0.0426
0.487400	350.009	308.872	−0.0102	0.0423
		$f(0, 3)$		
7.29063	350.007	306.257	0.0766	0.0724
6.00218	350.009	305.923	0.0526	0.0505
4.00125	350.010	306.393	0.0736	0.0476
1.98985	350.009	307.603	0.0486	0.0465
		$f(0, 4)$		
7.29062	350.006	306.021	−0.0008	0.1029
6.00219	350.009	305.915	0.0499	0.0725
4.00125	350.009	306.374	0.0676	0.0479
1.98984	350.006	307.574	0.0398	0.0685
		$f(1, 1)$		
7.41167	400.202	330.747	0.0241	0.0513
5.98076	400.197	329.733	0.0323	0.0481
4.00897	400.196	328.850	0.0238	0.0447
2.00091	400.193	328.524	−0.0083	0.0425
0.451922	400.202	328.787	−0.0042	0.0422
		$f(0, 3)$		
7.41118	400.202	330.789	0.0369	0.0656

p/MPa	T/K	c_{exp}/m s^{-1}	$100\left(\frac{c_{exp}-c_{EOS}}{c_{EOS}}\right)$	$U_c(c)$ c^{-1}/%
5.98038	400.197	329.824	0.0600	0.1462
4.00865	400.197	328.955	0.0556	0.0473
2.00079	400.193	328.688	0.0414	0.0522
		$f(0, 4)$		
7.41101	400.200	330.819	0.0461	0.0624
5.98038	400.197	329.886	0.0790	0.0670
4.00866	400.197	329.017	0.0746	0.0545
2.00078	400.191	328.635	0.0257	0.0678
		$f(1, 1)$		
7.26483	500.462	371.189	0.0079	0.0508
6.00866	500.462	369.692	0.0119	0.0481
4.00814	500.460	367.562	0.0030	0.0446
1.98838	500.459	365.732	−0.0241	0.0424
0.476588	500.502	364.753	−0.0093	0.0421
		$f(0, 3)$		
7.26441	500.462	371.243	0.0227	0.0527
6.00831	500.459	369.746	0.0268	0.0571
4.00792	500.462	367.673	0.0331	0.0468
1.98827	500.457	365.882	0.0172	0.0907
		$f(0, 4)$		
7.26437	500.462	371.283	0.0335	0.0543
6.00830	500.462	369.733	0.0230	0.1071
4.00791	500.461	367.608	0.0155	0.0734
1.98828	500.459	365.864	0.0121	0.1079

Table 4

Experimental (p, c, T, x) data in the vapor phase for a (0.25019 argon + 0.74981 carbon dioxide) mixture, relative deviations of the experimental data c_{exp} from speeds of sound c_{EOS} calculated with the EOS-CG equation of state of Gernert and Span [1], and the combined expanded uncertainty U_c ($k = 2$) of the speed of sound measurements are listed. p is the pressure and T is the temperature (ITS-90). The results for the non-radial mode $f(1, 1)$ and the radial modes $f(0, 3)$ and $f(0, 4)$ are tabulated individually. The standard uncertainty in temperature was less than 20 mK, the standard uncertainty in pressure was ($20 \cdot 10^{-6} \cdot p + 0.15$ kPa) for $p < 5$ MPa and ($20 \cdot 10^{-6} \cdot p + 1.0$ kPa) for $p > 5$ MPa, and the standard uncertainty in mixture composition was $4.4 \cdot 10^{-6}$ (mole fraction). Values written in italics indicate points that may have been affected by pre-condensation.

p/MPa	T/K	c_{exp}/m s^{-1}	$100\left(\frac{c_{exp}-c_{EOS}}{c_{EOS}}\right)$	$U_c(c)$ c^{-1}/%
		$f(1, 1)$		
5.50298	*276.088*	*227.574*	*−0.4944*	*0.0500*
5.39984	*276.090*	*228.574*	*−0.4344*	*0.0497*
5.29597	*276.092*	*229.564*	*−0.3796*	*0.0494*
4.99569	*276.092*	*232.298*	*−0.2616*	*0.0486*
4.00361	*276.088*	*240.290*	*−0.1853*	*0.0464*
1.99905	276.088	255.070	−0.0530	0.0431
0.501138	276.087	264.909	−0.0513	0.0424
		$f(0, 3)$		
5.29545	*276.092*	*229.019*	*−0.6179*	*0.0500*
4.99521	*276.092*	*231.832*	*−0.4635*	*0.0487*
4.00324	*276.089*	*240.293*	*−0.1854*	*0.0529*
1.99889	276.089	255.172	−0.0137	0.1122
		$f(0, 4)$		
5.50241	*276.089*	*226.977*	*−0.7579*	*0.0500*
5.39929	*276.090*	*227.997*	*−0.6878*	*0.0496*
5.29543	*276.092*	*229.011*	*−0.6215*	*0.0494*
4.99520	*276.091*	*231.822*	*−0.4676*	*0.0497*
4.00326	*276.088*	*240.282*	*−0.1898*	*0.0489*
1.99889	276.089	255.155	−0.0202	0.0495
		$f(1, 1)$		
8.05744	*290.014*	*227.741*	*−1.3363*	*0.0559*
6.01266	*290.008*	*240.255*	*−0.1374*	*0.0499*
4.02345	290.007	251.638	−0.0931	0.0458
1.97901	290.009	263.297	−0.0460	0.0429

p/MPa	T/K	c_{exp}/m s^{-1}	$100\left(\frac{c_{exp}-c_{EOS}}{c_{EOS}}\right)$	$U_c(c)$ c^{-1}/%
0.485294	290.008	271.437	−0.0459	0.0424
		$f(0, 3)$		
8.05710	*290.016*	*227.321*	*−1.5194*	*0.0598*
6.01191	*290.007*	*239.661*	*−0.3855*	*0.0501*
4.02312	290.007	251.707	−0.0664	0.0718
1.97886	290.009	263.375	−0.0168	0.0609
		$f(0, 4)$		
8.05704	*290.015*	*227.350*	*−1.5069*	*0.0558*
6.01213	*290.008*	*239.669*	*−0.3822*	*0.0522*
4.02313	290.007	251.647	−0.0903	0.0463
1.97886	290.009	263.408	−0.0041	0.0521
		$f(1, 1)$		
8.06330	*310.008*	*251.521*	*−0.2709*	*0.0541*
6.00022	310.007	258.015	−0.0772	0.0491
4.02418	310.009	265.613	−0.0191	0.0454
1.98105	310.008	274.006	−0.0259	0.0428
0.488279	310.008	280.301	−0.0305	0.0423
		$f(0, 3)$		
8.06271	*310.010*	*251.514*	*−0.2752*	*0.0588*
5.99962	310.005	258.004	−0.0818	0.0490
4.02386	310.008	265.675	0.0037	0.0550
1.98091	310.008	274.108	0.0110	0.0431
		$f(0, 4)$		
8.06253	*310.008*	*251.410*	*−0.3154*	*0.0552*
5.99973	310.007	257.987	−0.0887	0.0496
4.02388	310.009	265.669	0.0011	0.0548
1.98091	310.009	274.122	0.0160	0.0451
		$f(1, 1)$		
8.20098	350.013	282.123	−0.0345	0.0536
6.01823	350.011	284.804	−0.0003	0.0485
4.01058	350.011	288.505	0.0005	0.0449
1.98738	350.010	293.080	−0.0187	0.0426
0.500813	350.011	296.882	−0.0254	0.0422
		$f(0, 3)$		

p/MPa	T/K	c_{exp}/m s^{-1}	$100\left(\frac{c_{exp}-c_{EOS}}{c_{EOS}}\right)$	$U_c(c)$ c^{-1}/%
		$f(0, 4)$		
8.20028	350.013	282.089	−0.0464	0.0538
6.01776	350.011	284.820	0.0052	0.0492
4.01029	350.011	288.577	0.0255	0.0460
1.98725	350.010	293.211	0.0259	0.0591
		$f(0, 4)$		
8.20027	350.013	282.078	−0.0503	0.0603
6.01776	350.011	284.806	0.0002	0.0632
4.01027	350.010	288.520	0.0056	0.1061
1.98726	350.010	293.128	−0.0026	0.0650
		$f(1, 1)$		
7.95509	400.135	310.442	−0.0064	0.0526
6.01353	400.131	310.893	−0.0009	0.0483
4.01862	400.130	312.172	−0.0063	0.0448
1.98827	400.128	314.306	0.0106	0.0427
0.501932	400.127	316.145	−0.0232	0.0421
		$f(0, 3)$		
7.95441	400.131	310.439	−0.0067	0.0531
6.01312	400.131	310.980	0.0269	0.0502
4.01835	400.130	312.301	0.0351	0.0464
1.98814	400.129	314.380	0.0339	0.0630
		$f(0, 4)$		
7.95451	400.135	310.430	−0.0100	0.0701
6.01312	400.132	310.943	0.0152	0.0487
4.01835	400.130	312.247	0.0178	0.0729
1.98814	400.129	314.321	0.0153	0.0777
		$f(1, 1)$		
8.00803	500.486	353.784	−0.0067	0.0525
6.00121	500.484	352.393	−0.0111	0.0481
4.01028	500.483	351.501	−0.0117	0.0446
2.00405	500.481	351.027	−0.0238	0.0424
0.501805	500.480	350.997	−0.0246	0.0421
		$f(0, 3)$		
8.00752	500.486	353.817	0.0031	0.0539
6.00082	500.484	352.544	0.0318	0.0590

p/MPa	T/K	c_{exp}/m s^{-1}	$100\left(\frac{c_{exp}-c_{EOS}}{c_{EOS}}\right)$	$U_c(c)$ c^{-1}/%
4.01003	500.483	351.639	0.0277	0.0481
2.00394	500.481	351.192	0.0233	0.0442
		$f(0, 4)$		
8.00745	500.486	353.867	0.0170	0.0528
6.00081	500.484	352.488	0.0161	0.1095
4.01002	500.483	351.635	0.0266	0.0452
2.00394	500.481	351.234	0.0351	0.0499